Multiple failures in or around a stiff inclusion embedded in a soft matrix under a compressive loading

Daniel Quesada, Dominique Leguillon, Claude Putot

Multiple failures in or around a stiff inclusion embedded in a soft matrix under a compressive loading

Daniel Quesada, Dominique Leguillon, Claude Putot

PII: S0997-7538(09)00033-3
DOI: 10.1016/j.euromechsol.2009.03.001
Reference: EJMSOL 2509

To appear in: *European Journal of Mechanics A/Solids*

Received date: 23 January 2009
Accepted date: 6 March 2009

Please cite this article as: D. Quesada, D. Leguillon, C. Putot, Multiple failures in or around a stiff inclusion embedded in a soft matrix under a compressive loading, *European Journal of Mechanics A/Solids* (2009), doi: 10.1016/j.euromechsol.2009.03.001

Multiple failures in or around a stiff inclusion embedded in a soft matrix under a compressive loading

Daniel Quesada [a,b], Dominique Leguillon [a*], Claude Putot [b]

[a] *Institut Jean Le Rond d'Alembert, CNRS UMR 7190, Université P. et M. Curie, case 162, 4 place Jussieu, 75252 Paris Cedex 05, France.*
[b] *IFP, Direction Mécanique Appliquée, 1&4 avenue de Bois-Préau, BP311, 92506 Rueil Malmaison Cedex, France.*

[*] Corresponding author, IJLRA, University P. and M. Curie, case 162, 4 place Jussieu, 75252 PARIS CEDEX 05, France – tel.: +33(0)144 275 322, fax: +33(0)144 275 259
e-mail : dominique.leguillon@upmc.fr

Running title: **Multiple failures**

Abstract

As well as cavities, embedded concretions and fossil inclusions are known to be possible sites of fracture initiation in rocks under compressive loadings. Parallel cracks can be observed in stiff inclusions surrounded by soft sediments. The crack spacing is often small and strictly incompatible with a mechanism of successive failures and reloading because of a shielding effect. The explanation proposed here is that these failures occur almost simultaneously thus avoiding this effect. A mixed criterion developed by one of the authors and involving both energy and stress conditions is able to predict such a fracturing mechanism. It is strongly related to a size effect: the larger the inclusion diameter, the higher the number of cracks. There is a competition between this mechanism and other fracture events like matrix failure or interface debonding. It is shown that, depending on the material properties and the concretion size, one of them can become predominant.

Keywords: brittle fracture, crack nucleation, compressive stress, rock inclusions

1. Introduction

Rigid inclusions (concretions, fossil inclusions) embedded in a soft sedimentary matrix are known to be potential sites for the initiation of cracks. Bessinger et al. (2003) have studied a group of limestone concretions in a sandstone bed on Vancouver Island (British Columbia) and observed different configurations. Concretions are characterized by their size and the contrast of their mechanical properties with the surrounding matrix. The failure occurs either in the sandstone matrix in the vicinity of the concretion, or at the interface between concretion and sandstone, or even inside the concretion with one or more parallel cracks (figures 1.a and 1.b). The best example is a 50 cm concretion with 5 closely spaced cracks (figure 1.a).
Eidelman and Reches (1992) have made similar comments on pebbles included in a weakly cemented matrix found in two different sites in California and Israel. The material varies from one pebble to another: gneiss, granite, slate, sandstone or limestone. Most of the ellipsoidal to spherical pebbles are 10 to 30 cm in diameter, and contain 2 to 5 closely spaced parallel cracks. They report that the number of cracks increases with the size of the pebbles.

Moreover, they note that the pebbles are preferentially fractured, but that fractures may extend in some cases into the matrix (figures 1.c and 1.d). Within pebbles, the crack extensions do not seem to be influenced by the heterogeneity of the material.

In the two cases, the inclusions are more rigid than the matrix. Both studies indicate a higher density of cracks inside or near inclusions than elsewhere in the matrix. The constant crack alignment in concretions and in the matrix indicates that the failure mechanisms occurred during the same tectonic episode. The authors' point of view is that the fracturing origin lies in a tectonic compression combined with a significant pore pressure leading to a low confinement and thus an almost pure uniaxial compressive state. In particular, Bessinger et al. (2003) find that, in the case of multiple cracks, the low spacing (much lower than the concretion diameter) is incompatible with a remote tension and the resulting shielding effect between cracks. The compressive stress plays an essential role in their nucleation. Lorenz et al. (1991) also analyze mechanical stress amplification in a lenticular sandstone inclusion in limestone. Once again compression is invoked to explain the observations.

It must be pointed out that the two previous analyses differ, but the final results coincide on many points. The Eidelman and Reches (1992) model uses the analytical approach of Eshelby (1957) to compute the stress field within the inclusion as a function of the mechanical properties of the materials and the remote load. Eidelman and Reches (1992) then use a maximum tensile stress condition to predict the appearance of a single crack in the inclusion. Bessinger et al. study the mechanism of multiple fractures of the concretion numerically, under either a tensile or a compressive loading. For them, the multiple failures occur in successive steps. In case of a tensile loading, decohesion of the interface is supposed to intervene first, it prevents the breakdown of the concretion. Thus, only a sub-critical growth due to a humid or chemically reactive environment, could justify the existence of internal cracks. In the sub-critical mode, cracks grow very slowly and under a remote load far less than those observed in an inert environment where fracture is unstable and cracks grow at speeds which are comparable to the elastic waves speed. The critical stress intensity factor K_{Ic} (see eqn. (2)), obtained in laboratories, reflects these latter conditions. For in situ conditions, the sub-critical growth rate v of a crack can be written (at least for a given range of the stress intensity factor (SIF) K_I): $v = A(K_I / K_{Ic})^p$ following a fatigue-like power law (Olson 2004). Here A is a scaling coefficient, and p is the sub-critical index. The value of p varies considerably depending on the kind of rock and environment, from 20 for sandstone immersed into water to over 250 in dry for carbonates (Olson 2004). Nevertheless, following Bessinger et al., the values of p necessary to propagate multiple fractures should be lower by several orders of magnitude than those obtained experimentally, and these values have never been found in rocks. Thus multiple cracking in concretions seems unlikely to occur according to this mechanism.

The remote tension can play a role in some specific configurations. This is the case proposed by Lash and Engelder (2007), for example, who observe fractures appearing on the outer arc of a folding zone in the Appalachians. In this study, which also contains some examples of fractures inside or near concretions, fracturing is linked to an extension in the perpendicular direction to the fracture and/or thermal shrinkage in the early stages of the tectonic cycles. But it must be noted that crack spacing is larger and so more compatible with the hypothesis of a remote tension (Mandl 2005).

Other publications offer examples of fracturing inside or near rigid inclusions. McConaughy and Engelder (1999) show an example of cracks in the matrix on both sides of two concretions (figure 1.e) in the region of New York. They refer to the mechanisms mentioned just above, although the spacing between cracks is, from our point of view, incompatible with such mechanisms.

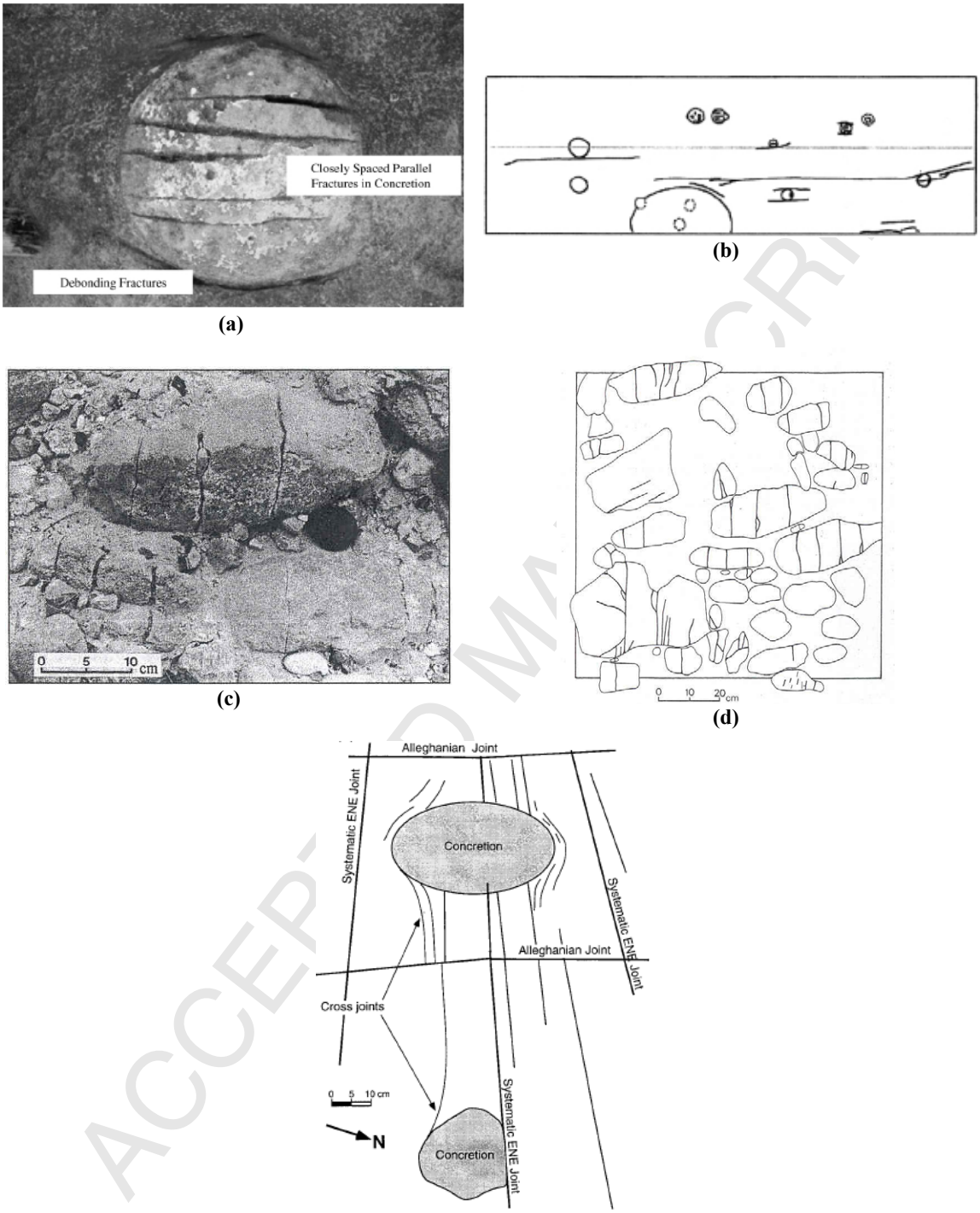

Figure 1. Cracks inside or in the vicinity of concretions: **(a)** 5 closely spaced cracks in a concretion (Bessinger et al. 2003); **(b)** overview of cracks inside and around concretions in a sandstone matrix, (Bessinger et al. 2003) ; **(c)** multiple cracks in a pebble (Eidelman and Reches 1992) ; **(d)** various kinds of failure in pebbles (Eidelman and Reches 1992) ; **(e)** matrix cracking in the vicinity of two concretions (Mc Conaughy and Engelder 1999).

Another approach able to provide an explanation to the multiple cracking of an inclusion is proposed herein. It is based on a mixed criterion involving both energy and stress conditions

(Leguillon 2002). Starting from an energy balance between an elastic initial state prior to any crack onset and after the appearance of a new crack or a crack extension with surface δS leads to the following inequality

$$-\frac{\delta W_p}{\delta S} = G \geq G_c \tag{1}$$

where δW_p is the change in potential energy and G_c the material toughness (J.m^{-2}) which can also be expressed in terms of the critical mode I stress intensity factor K_{Ic} (MPa.m$^{1/2}$), also called toughness, using the Irwin relation (E and ν are respectively the Young modulus and the Poisson ratio of the material)

$$G_c = \frac{1-\nu^2}{E} K_{Ic}^2 \tag{2}$$

Inequality (1) is an unquestionable necessary condition for failure, G is the incremental energy release rate which involves a crack increment δS. Note that the Griffith criterion derives from (1) at the limit as $\delta S \to 0$.
On the other hand, the maximum tensile stress criterion is based on the maximum tension that a material can bear. Failure occurs at a point if

$$\sigma \geq \sigma_c \tag{3}$$

where σ holds for the tension orthogonally to the failure direction and σ_c for the tensile strength of the material.
Nevertheless, the crack nucleation cannot be correctly predicted by either of these two usual brittle fracture criteria. They give contradictory results and neither one nor the other agrees with the experiments (Leguillon 2002).
Within the plane strain assumption, a lower bound for admissible crack length is derived from (1) whereas (3) leads to an upper bound. The compatibility between these two bounds allows a critical nucleation length to be defined. The crack is assumed to jump this length at initiation. Inserting this critical length in (1) or equivalently in (3) leads to a nucleation criterion taking into account both conditions (1) and (3). It has already proved its efficiency in various situations (Leguillon 2002, Leguillon et al. 2007).
The interaction between this critical length and the concretion diameter is responsible for a strong size effect playing a prominent role in the crack nucleation and the number of cracks appearing within a concretion.

2. The model and the matched asymptotics procedure

The geometry used in the present model is shown in figure 2. A stiff circular inclusion with diameter d is embedded in a more compliant matrix and submitted to a uniaxial compressive loading σ_∞ (using mechanical notations σ_∞ is negative, thus throughout the paper results are given in terms of $|\sigma_\infty|$). The diameter d is assumed to be small compared to the specimen size, making it possible for an asymptotic expansions approximation in terms of the small parameter d. Thereafter, $E^{(i)}$ and $\nu^{(i)}$ (resp. $E^{(m)}$ and $\nu^{(m)}$) denote the Young modulus and the Poisson ratio of the inclusion (resp. the matrix).

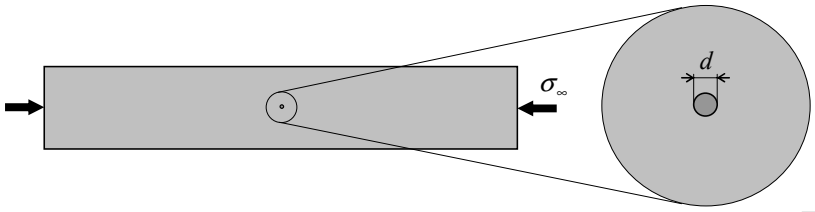

Figure 2. The domain Ω^d made of a small stiff inclusion embedded in a compliant matrix and submitted to a uniaxial compressive loading σ_∞.

Solving numerically an elasticity problem in the domain Ω^d (figure 2) embedding a small inclusion with diameter d presents some difficulties because of the small size of the perturbation which requires a drastic finite element (FE) mesh refinement in its vicinity especially if additional inside or neighbouring cracks must be taken into account. It is better trying to represent the elastic solution $\underline{U}^d$ in the following approximate form called outer expansion

$$\underline{U}^d(x_1,x_2) = \underline{U}^0(x_1,x_2) \text{ + small correction} \tag{4}$$

where $\underline{U}^0$ is the solution to the same elasticity problem, but now posed on the unperturbed domain Ω^0 (figure 3.a) which can be considered as the limit of Ω^d as $d \to 0$. In other words, the small inclusion is not visible. It is the classical simplified frame often used to perform FE computations since the meshing procedure prevents taking into account very small details.

It is clear that this solution $\underline{U}^0$ is a satisfying approximation of $\underline{U}^d$ away from the perturbation, i.e., outside a neighbourhood of the perturbation, and hence its designation as the outer field (or far field).

Obviously, this information is incomplete, particularly when we are interested in the fracture mechanisms that can occur in or around the inclusion. To this aim, the space variables are stretched introducing the change of variables $y_i = x_i / d$. In the limit when $d \to 0$, we obtain an unbounded domain Ω^∞ (looking like the enlarged frame in figure 3.b) in which the inclusion diameter now equals 1.

We then search for another representation of the same solution under the form of an expansion known as inner expansion and describing the near field

$$\underline{U}^d(x_1,x_2) = \underline{U}^d(dy_1,dy_2) = F_0(d)\,\underline{V}^0(y_1,y_2) + F_1(d)\,\underline{V}^1(y_1,y_2) + \ldots \tag{5}$$

where $F_1(d)/F_0(d) \to 0$ as $d \to 0$. Substituting this expression in the equations of the elastic problem leads to problems in the new unknown functions $\underline{V}^0$, $\underline{V}^1$, but where conditions at infinity lack having correctly stated problems. These missing conditions derive from the matching procedure.

The inner and outer expansions describe the solution $\underline{U}^d$ in terms of near and far fields. An intermediate zone (close to the perturbation for the far field and far from it for the near field) must exist where both expansions are valid. In other words, the behaviour of the far field, when one comes closer to the origin, must match with the behaviour of the near field, when one moves away from the perturbation.

The behaviour of the far field near the origin, is simply described by the uniaxial compressive state

$$\underline{U}^0(x_1,x_2)=\underline{U}^0(r,\theta)=\sigma_\infty r\underline{t}(\theta) \tag{6}$$

It is written here using the polar coordinates r and θ to bring into evidence the linear dependency in r which intervenes in the matching procedure. The stress field associated to the displacement $r\underline{t}(\theta)$ fulfils $\sigma_{11}=1$, $\sigma_{12}=\sigma_{22}=0$.

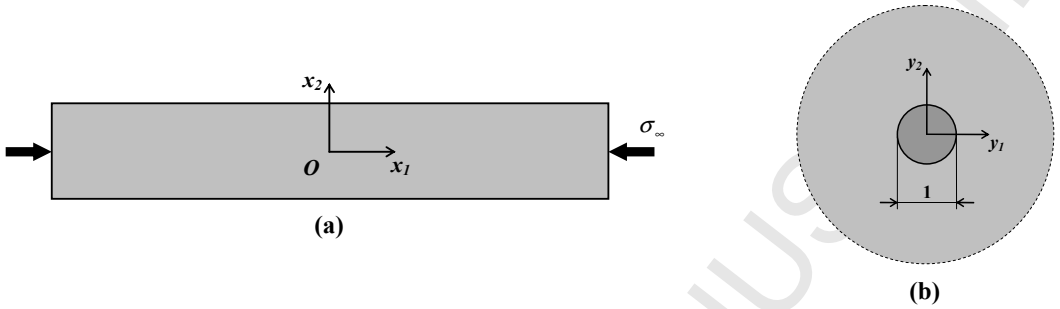

Figure 3. The two scales and the two domains of the matched asymptotic expansions process: **(a)** the outer domain Ω^0 (the perturbation is not visible); **(b)** the unbounded inner domain Ω^∞ (the concretion diameter equals 1 and boundaries are thrown to infinity).

The matching conditions are written as follows

$$F_0(d)\ \underline{V}^0(y_1,y_2)\ \approx\ 0\ ;\ \ F_1(d)\ \underline{V}^1(y_1,y_2)\ \approx\ \sigma_\infty d\ \rho\ \underline{t}(\theta) \tag{7}$$

when $\rho=r/d=\sqrt{y_1^2+y_2^2}\ \to\infty$ (the symbol $\approx$ means "behaves like at infinity"), thus it comes straightforwardly

$$F_0(d)=1\,,\ \underline{V}^0(y_1,y_2)=0\,;\ F_1(d)=\sigma_\infty d\ \text{ and }\ \underline{V}^1(y_1,y_2)\approx\rho\underline{t}(\theta) \tag{8}$$

The most significant term $\underline{V}^1$ is the solution to a problem that can be solved using a superposition principle (Leguillon and Sanchez-Palencia 1987, Leguillon 2002). The expansion of the actual solution $\underline{U}^d$ and the associated stress field become

$$\underline{U}^d(x_1,x_2)=\underline{U}^d(dy_1,dy_2)=\sigma_\infty d\ \underline{V}^1(y_1,y_2)+... \tag{9}$$

$$\underline{\underline{\sigma}}(\underline{U}^d(x_1,x_2))=\sigma_\infty\underline{\underline{\tilde{\sigma}}}(\underline{V}^1(y_1,y_2))+... \tag{10}$$

where $\underline{\underline{\sigma}}(\underline{U}^d)=C:\nabla_x^s(\underline{U}^d)$ and $\underline{\underline{\tilde{\sigma}}}(\underline{V}^1)=C:\nabla_y^s(\underline{V}^1)$ express the elastic constitutive law (here ∇_x^s (resp. ∇_y^s) denotes the symmetric part of the gradient with respect to x (resp. to y) and C the stiffness matrix function of the Young modulus and the Poisson ratio of the material under consideration, i.e. inclusion or matrix).

3. The tensile stress field orthogonal to the remote compressive loading

A preliminary study is carried out to determine the potential sites for crack nucleation. We assume that the expected cracks are parallel to the compressive remote load and nucleate at locations where the tensile stress is maximum.

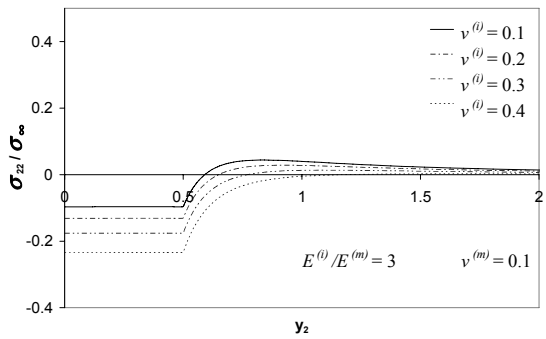

(a)

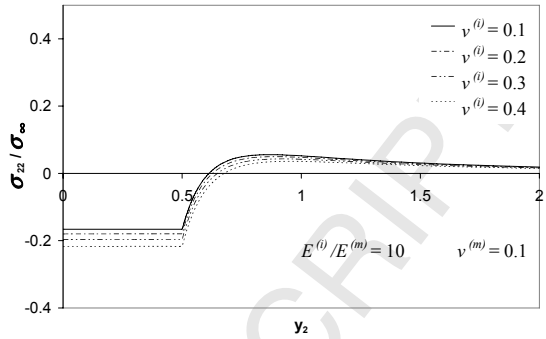

(b)

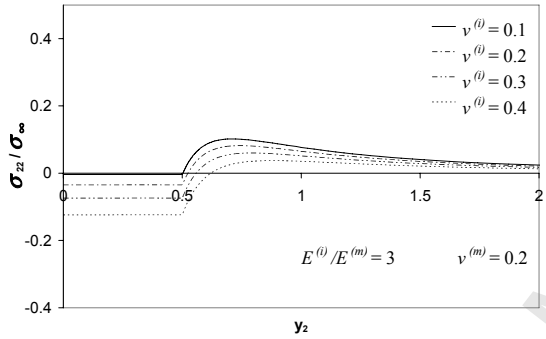

(c)

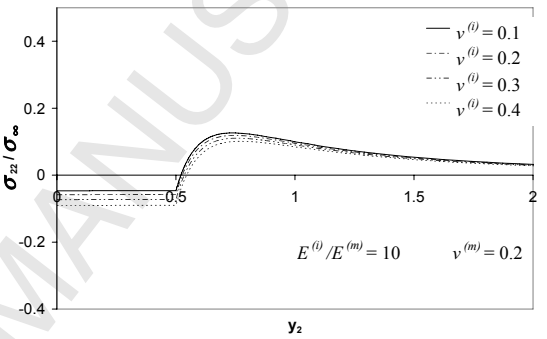

(d)

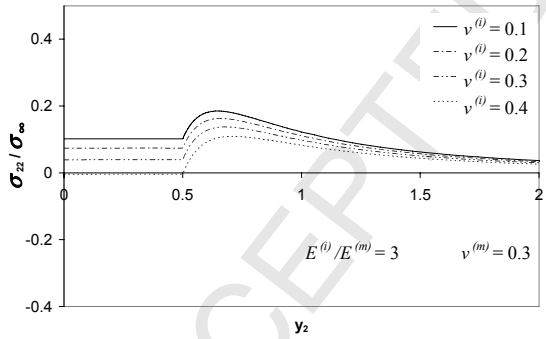

(e)

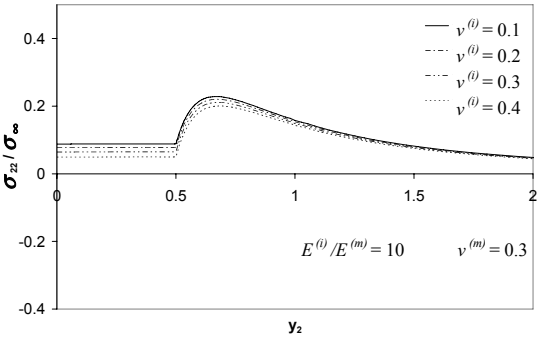

(f)

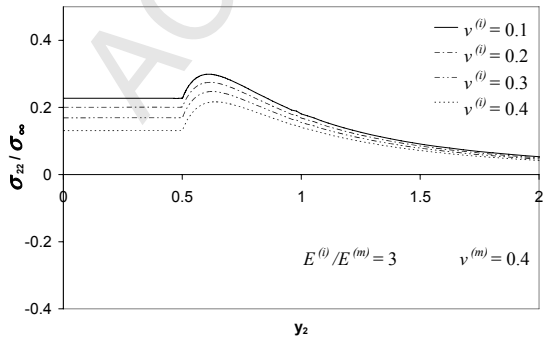

(g)

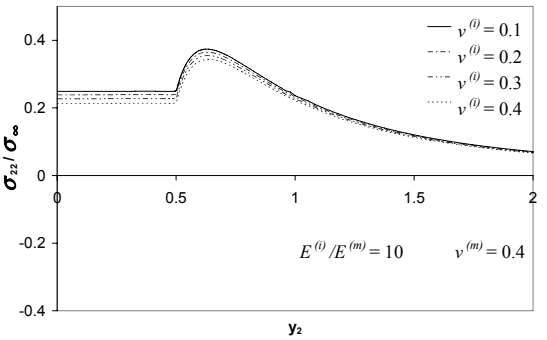

(h)

Figure 4. Dimensionless opening component $\tilde{\sigma}_{22} = \sigma_{22} / \sigma_{\infty}$ function of y_2 at $y_1 = 0$ for different elastic moduli ratios between matrix and concretion.

Figure 4 plots the opening component $\tilde{\sigma}_{22}$ along the y_2 axis at $y_1 = 0$ (see figure 3.b), for different values of $\nu^{(m)}$ and $\nu^{(i)}$ and for two different stiffness contrasts $E^{(i)} / E^{(m)} = 3$ and $E^{(i)} / E^{(m)} = 10$. The matrix Poisson ratio $\nu^{(m)}$ plays a crucial role whereas that of $\nu^{(i)}$ is less pronounced, but still significant for low contrasts $E^{(i)} / E^{(m)}$.
Of course, the computed value for $\tilde{\sigma}_{22}$ in the concretion agrees perfectly with the analytical approach of Eshelby (1957) cited by Eidelman and Reches (1992).

According to the observations, three mechanisms can occur: concretion failure, matrix failure and interface debonding. They are first studied separately and then the competition between them is analysed.

4. Inclusion failure

As previously mentioned, the case of multiple fractures in rigid inclusions has been observed by several authors (Eidelman and Reches 1992; Bessinger et al. 2003). The picture in figure 1.a (Bessinger et al. 2003) shows five parallel cracks in a limestone concretion included in a sandstone bank. The spacing between the fractures is low and strictly incompatible with a sequential failure mechanism where a shielding effect prevents any small spacing between cracks. A possible explanation is that these failures have occurred almost simultaneously and so avoided this shielding effect. The mixed criterion, involving both tension and energy conditions, allows such a mechanism to be described. It brings into evidence a strong size effect due to the inclusion diameter.
According to figures 4.e to 4.h, the inside crack initiation requires a high Poisson's ratio of the matrix $\nu^{(m)}$, typically $\nu^{(m)} \geq 0.3$ in order to have a positive tension in the concretion. The Poisson's ratio $\nu^{(i)}$ of the inclusion has a significant influence on the opening stress component only for low stiffness contrasts $E^{(i)} / E^{(m)}$. A high $\nu^{(m)}$ and a low $\nu^{(i)}$ is the most favourable situation for failure within the concretion.
The opening stress is constant through the inclusion. As a consequence, any point is a potential site for nucleation; and the stress condition for failure is simultaneously fulfilled at all points of the presupposed crack paths. An upper bound for admissible crack lengths does not exist. This implies that if a crack starts, it goes brutally through the whole concretion provided the energy condition is also verified. Nevertheless, cracks cannot extend outside because the matrix ahead is in a compressive state. Moreover, one or more horizontal cracks are likely to occur within the concretion if the available stored energy is sufficiently high. The brutal failure could partly explain why the crack extensions are not strongly influenced by heterogeneities inside the pebbles as pointed out by Eidelman and Reches (1992).
For simplicity, we assume that the cracks are regularly distributed within the inclusion as illustrated in figure 5. In each case the dimensionless crack length at initiation $\mu_0 = \ell_0 / d$ is known; it is the sum of the lengths of the different cracks (whereas this length is a priori unknown in the general case of application of the mixed criterion, see sections 7 and 8).

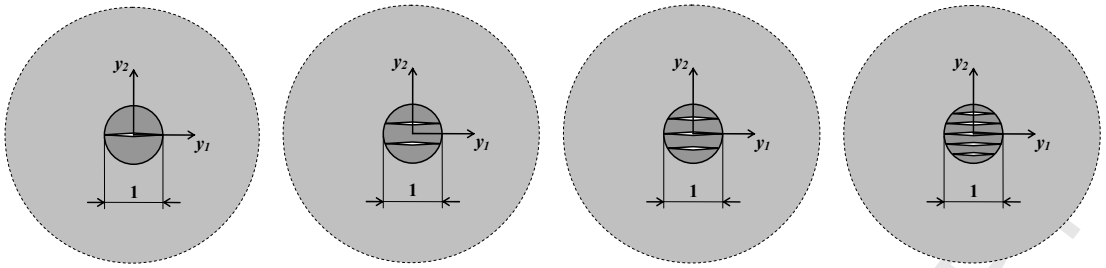

Figure 5. Inner domains in different cases: from 1 to 5 cracks within the concretion.

The initial (uncracked) and final (totally cracked) configurations are the only ones involved in calculating the incremental energy release rate G. Expansion (9) holds in the uncracked case (i.e. $\ell_0 = 0$ where ℓ_0 denotes the cracks' total length, see eqn. $(11)_1$ equivalent to (9)). The cracked case can be described as well (eqn. $(11)_2$), changing the inner domain by adding a single or many cracks as shown in figure 5

$$\begin{cases} \underline{U}^d(x_1,x_2,0) & = \underline{U}^d(dy_1,dy_2,0) & = \sigma_\infty d\ \underline{V}^1(y_1,y_2,0)+... \\ \underline{U}^d(x_1,x_2,\ell_0) & = \underline{U}^d(dy_1,dy_2,d\mu_0) & = \sigma_\infty d\ \underline{V}^1(y_1,y_2,\mu_0)+... \end{cases} \tag{11}$$

where $\mu_0 = \ell_0 / d$ is the dimensionless cracks' total length. This leads to the condition (12) following a strictly analogous approach to that used in Leguillon et al. (2007) in the case of crack nucleation at poles of a cavity under a compressive loading

$$G(\ell_0) = \frac{W_p(\ell_0) - W_p(0)}{\ell_0} = \frac{W_p(\ell_0) - W_p(0)}{\mu_0 d} = \sigma_\infty^2\ d\ B_n(\mu_0) \geq G_c^{(i)} = K_{Ic}^{(i)2}(1-\nu^{(i)2})/E^{(i)} \tag{12}$$

The scaling coefficient B_n depends on the number n of cracks (through μ_0) and on the cracks' location, but not on the overall geometry of the structure or the load intensity. It can be extracted, once and for all for each n, from a finite element approximation of $\underline{V}^1(y_1,y_2,\mu_0)$ by a path-independent integral (Leguillon and Sanchez-Palencia 1987, Leguillon et al. 2007).

According to (10) the stress condition is written as follows

$$\sigma_{22} = \sigma_\infty \tilde{\sigma}_{22} \geq \sigma_c^{(i)} \tag{13}$$

Figure 6 gives the load at failure σ_∞ and the number n of cracks in the inclusion functions of the inclusion diameter d in the case: $\nu^{(i)} = 0.1$, $\nu^{(m)} = 0.4$, $\sigma_c^{(i)} = 5\,\text{MPa}$ and $K_{Ic}^{(i)} = 1\text{MPa.m}^{1/2}$. It evidences the size effect and especially the influence of the concretion diameter d on the number of nucleating cracks.

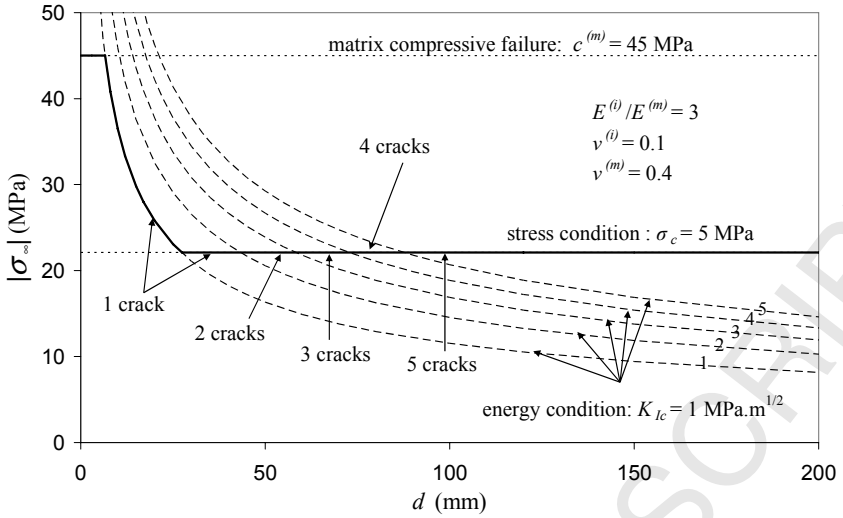

Figure 6. Critical load at initiation $|\sigma_\infty|$ and number n of cracks (from 1 to 5) in the inclusion, functions of the inclusion diameter d. The predicted value $|\sigma_\infty|$ is bounded from above by the matrix compressive strength $c^{(m)}$.

As mentioned above, the mixed criterion merges two necessary conditions. The energy condition depends on d, as well as on the number n of cracks in the concretion (through the parameter B_n), whereas the stress condition is independent of n and d (horizontal line in figure 6). In the present case where μ_0 is a priori known, the two conditions are uncoupled.

- For very small inclusion size, the compressive strength $c^{(m)}$ = 45 MPa of the matrix is reached prior to any other mechanism.
- For the inclusion size immediately below, the energy condition for a single crack governs the mechanism $\sigma_\infty = \sqrt{G_c^{(i)} / d\ B_1}$ and $\sigma_\infty > \sigma_c / \tilde{\sigma}_{22}$. The diameter d for which equality holds in the two cases is the limit of a new regime governed by the stress condition $\sigma_\infty = \sigma_c / \tilde{\sigma}_{22}$.
- As d increases, the gap between the two conditions grows and a significant amount of extra energy becomes available. Then the horizontal line $\sigma_\infty = \sigma_c / \tilde{\sigma}_{22}$ meets the energy condition for two cracks $\sigma_\infty = \sqrt{G_c^{(i)} / d\ B_2}$, etc.

The number of cracks increases with the concretion size as observed by Eidelman and Reches (1992).

5. Sensitivity of the model to various parameters

In the present case the stress and energy conditions are uncoupled as mentioned in the previous section. Thus the sensitivity to the failure parameters σ_c and $K_{Ic}^{(i)}$ is trivial. This is illustrated in figure 7.a. The next figure, 7.b, shows the sensitivity of the criterion to the Young moduli contrast between inclusion and matrix.

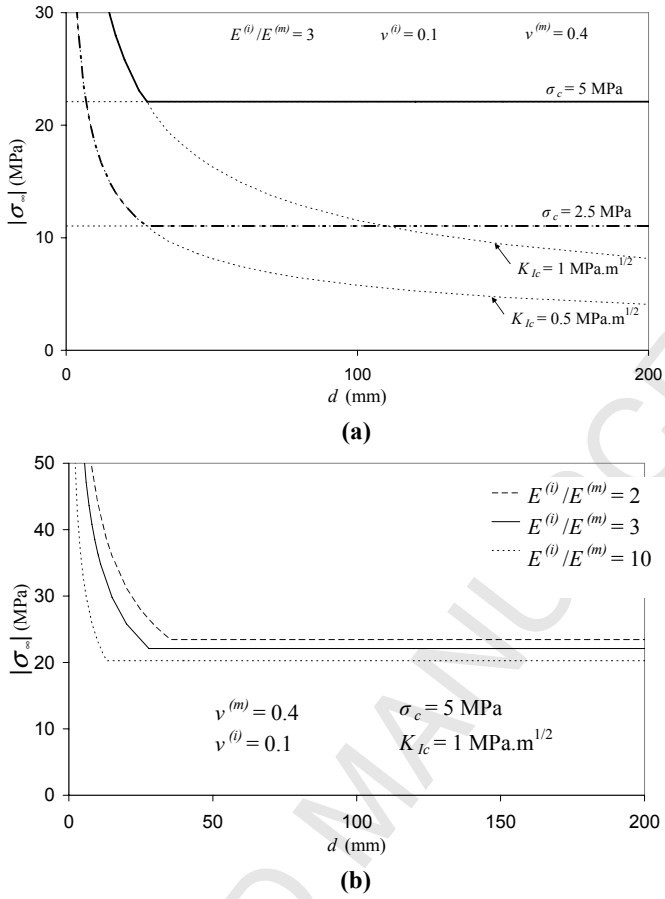

Figure 7. Sensitivity of the model for a single crack; **(a)** to the failure parameters. The solid line (resp. dotted/dashed line) corresponds to the mixed criterion with $\sigma_c^{(i)} = 5\,\text{MPa}$ and $K_c^{(i)} = 1\,\text{MPa.m}^{1/2}$ (resp. $\sigma_c^{(i)} = 2.5\,\text{MPa}$ and $K_c^{(i)} = 0.5\,\text{MPa.m}^{1/2}$); **(b)** to the stiffness contrast $E^{(i)}/E^{(m)}$ between inclusion and matrix.

6. Comparison with data

Let us consider the concretion failure observed by Bessinger et al. (2003) and shown in figure 1.a. The tensile strength of the concretion $\sigma_c^{(i)} = 18\,\text{MPa}$ is determined by a Brazilian test on samples taken from three different concretions of the same type. No specific test is performed to obtain the value of $K_{Ic}^{(i)}$. The Young moduli and Poisson ratios are also determined experimentally, but according to Bessinger et al., their values as well as the tensile strength are probably overestimated by the experimental set-up. Moreover, there is another fundamental uncertainty: should we use the current values of the mechanical parameters? Bessinger et al. computations and the present ones give much better results if the parameters' values are considered to be those during the materials' consolidation stage. For a concretion diameter $d = 50\,\text{cm}$ and 5 observed cracks, assuming the toughness value $K_{Ic}^{(i)}$ between 1 and 3 MPa.m$^{1/2}$, the tensile strength $\sigma_c^{(i)}$ appears to lie between 2 and 7.5 MPa, which seems to be quite reasonable. These multiple fractures can be a good indicator of a palaeostress state.

7. Matrix failure

The curves in figure 4 show that σ_{22} is positive in the matrix whatever the mechanical characteristics of the two materials, except in some cases at close proximity to the inclusion. Failure of the matrix can therefore a priori take place in all cases. We assume that the direction of nucleating cracks is once again parallel to the remote load (i.e. parallel to the y_1 axis). The peak of tension is clearly visible on the graphs of figure 4. Excluding some particular cases of figure 4(a), it lies in most cases between $y_2 = 0.6$ and $y_2 = 0.8$, depending on the stiffness contrast $E^{(i)} / E^{(m)}$ and on the Poisson ratios $\nu^{(i)}$ and $\nu^{(m)}$.
In the sequel, we analyze the particular case $E^{(i)} / E^{(m)} = 3$, $\nu^{(m)} = 0.4$ and $\nu^{(i)} = 0.1$. By symmetry two cracks are likely to nucleate horizontally, on both sides of the concretion at $y_2 = \pm 0.61$ (figure 8). Note that this distribution of fractures is very similar to that observed by McConaughy and Engelder (1999) (figure 1.e).

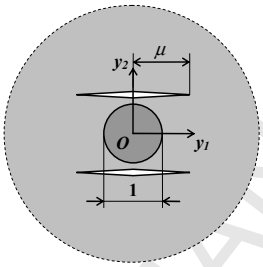

Figure 8. Inner domain associated with the matrix failure.

Thanks to the mixed criterion, we can determine the critical remote load σ_∞ at nucleation of these two cracks; each of them having a dimensionless length $2\mu_0$ (figure 8). Contrary to the previous case (failure inside the concretion, section 4) where the crack length at initiation was known in advance due to the constant opening stress field in the concretion, this length is a priori unknown here.
A finite element computation in the uncracked configuration allows the opening stress component $\tilde{\sigma}_{22}(\mu)$ along the presupposed crack path (figure 9.a) to be determined. It is a decreasing function of μ. Fulfilling the stress condition provides an upper bound μ_{01} of the admissible dimensionless cracks' half length.
Then the energy release rate $G(\mu)$, a function of the dimensionless cracks half length μ, is calculated by successively unbuttoning the nodes along the presupposed crack path. It is an increasing function of μ. Thus the energy condition provides a lower bound μ_{02} (figure 9.b). For a low remote load these two bounds are incompatible. Increasing the remote load makes it possible to merge these two values to obtain $\mu_0 = \mu_{01} = \mu_{02}$, which is the characteristic nucleation dimensionless half length. The associated remote load σ_∞ is the critical remote load at failure.

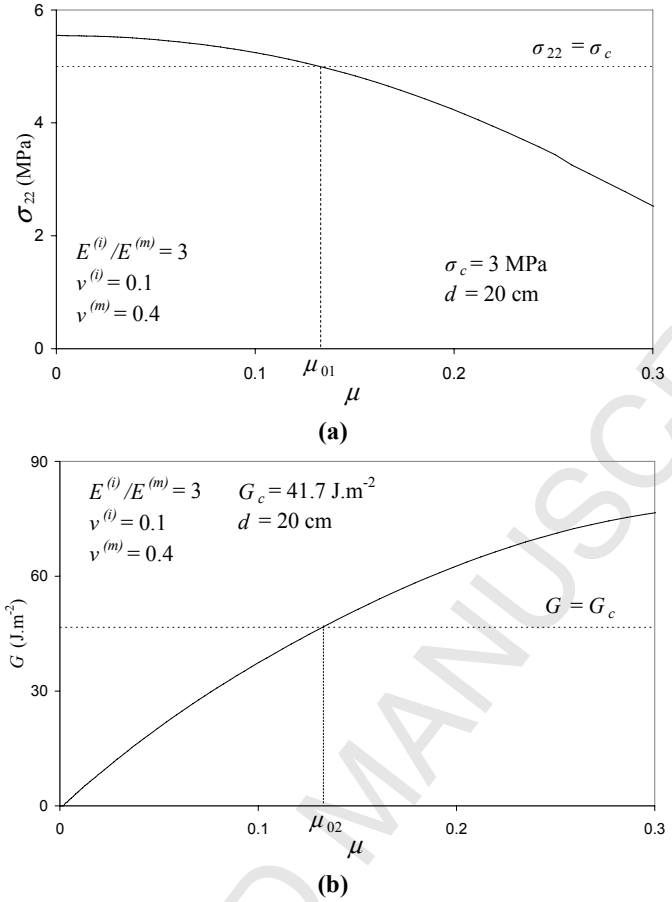

Figure 9. **(a)** Opening stress component σ_{22} along the presupposed crack path, in the uncracked structure; **(b)** energy release rate G calculated for two cracks with dimensionless half length μ. The remote load $|\sigma_\infty|$ for which $\mu_{01} = \mu_{02}$ is the critical load at failure.

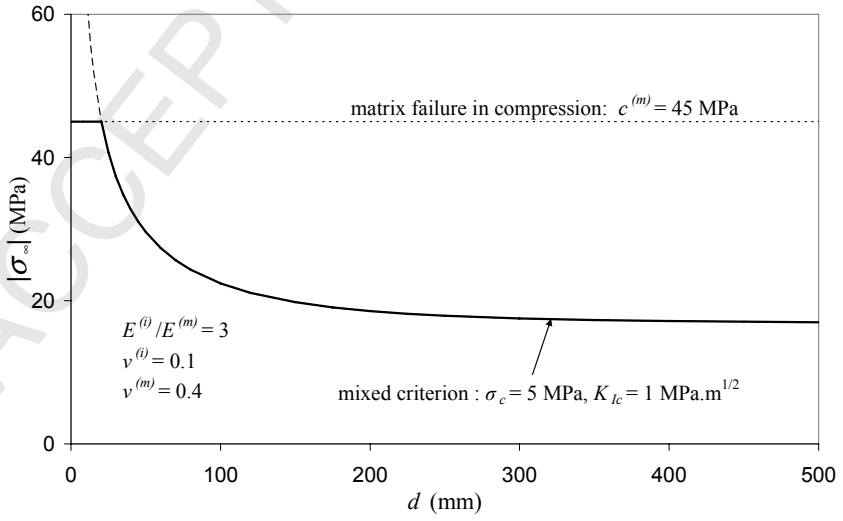

Figure 10. Critical remote load $|\sigma_\infty|$ function of the inclusion diameter d. The predicted value $|\sigma_\infty|$ is bounded from above by the matrix compressive strength $c^{(m)}$.

Once again, these curves exhibit a significant size effect due to the inclusion diameter d ; the larger the inclusion, the lower the critical remote load at failure. The critical load becomes almost constant for large inclusions (figure 10). For very small inclusions, the critical value of σ_∞ is bounded from above by the matrix compressive strength $c^{(m)}$.

A sensitivity analysis to the parameters $\sigma_c^{(m)}$ and $K_{Ic}^{(m)}$ is illustrated in figure 11. The role of the matrix toughness $K_{Ic}^{(m)}$ is significant for small inclusions whereas that of $\sigma_c^{(m)}$ becomes more significant for large ones. In other words, the energy condition is more predominant for small inclusions, whereas the stress condition takes precedence for large inclusions.

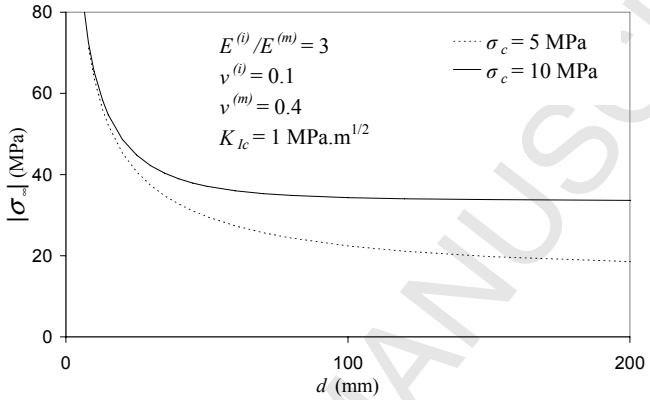

(a)

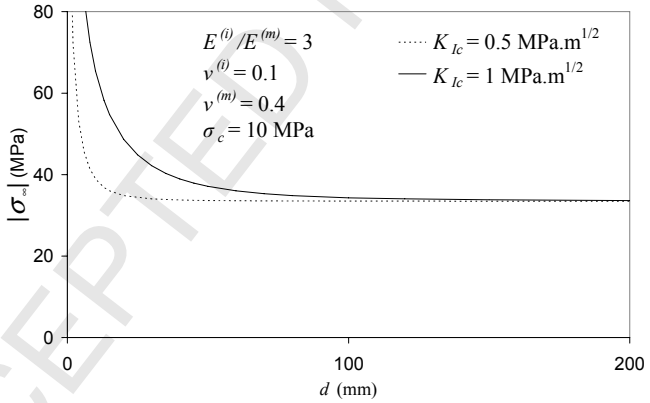

(b)

Figure 11. Sensitivity to the matrix failure parameters: **(a)** to $\sigma_c^{(m)}$; **(b)** to $K_{Ic}^{(m)}$.

8. Interface debonding

The matrix/inclusion interface debonding is another possible mechanism (figure 12). The prediction method of the critical load at failure σ_∞ remains strictly identical to that of the matrix failure. The only difference is that the stress component to be considered is no longer σ_{22} but the radial component σ_{rr} associated with the opening of the interface. It reaches a maximum at $y_1 = 0$. The curves $\sigma_{rr}(\mu)$ and $G(\mu)$ are very similar to those exhibited in figure 9 and the same reasoning applies.

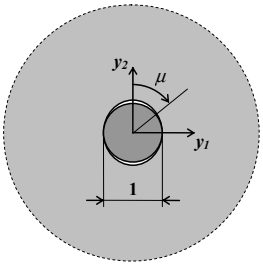

Figure 12. Inner domain associated with the interface debonding.

Indeed, the main difficulty here lies in the knowledge of the failure parameters of the interface: $K_{Ic}^{(d)}$ and $\sigma_c^{(d)}$ which would require very specific experimental tests. We consider two cases. In the first one, the smallest of the two materials' brittleness is selected. In case of interface debonding, this is a reasonable choice; otherwise if the interface was stronger then failure would not occur along the interface but within the most brittle material. In the second case, the interface properties are arbitrarily set at half those of the previous case.

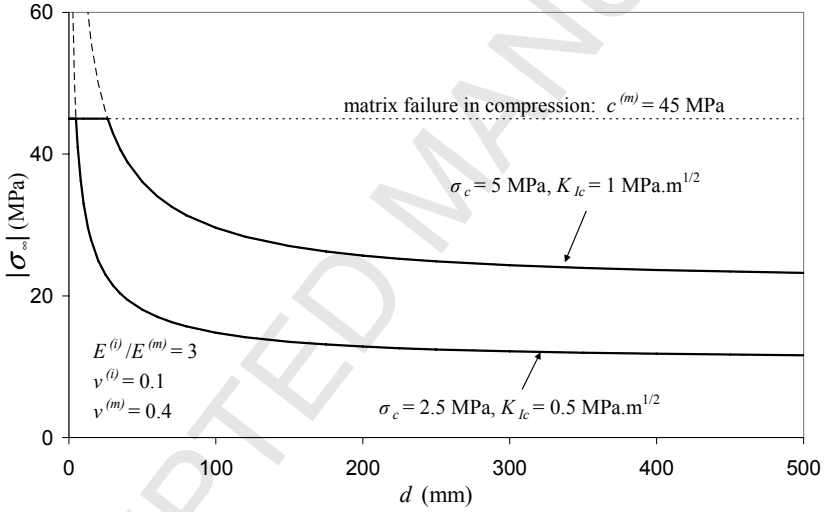

Figure 13. Remote critical load σ_∞ at interface debonding function of the inclusion diameter d. As previously mentioned this value is bounded from above by the matrix compressive strength $c^{(m)}$.

Once again, there is a strong size effect due to the diameter d on the critical remote load at interface debonding (figure 13). Moreover, the sensitivity of the model to the different failure parameters remains almost the same as that encountered for the matrix failure.

9. Competition between the different mechanisms

As in the previous sections, the elastic moduli of the two materials are set at: $E^{(i)}/E^{(m)} = 3$ MPa, $\nu^{(m)} = 0.4$ and $\nu^{(i)} = 0.1$. The different curves (6), (10) and (13) are superimposed on the same graph (figure 14) with the following failure parameters:

- matrix : $\sigma_c^{(m)} = 4\,\text{MPa},\ K_{Ic}^{(m)} = 1.8\,\text{MPa.m}^{1/2}$.
- interface : $\sigma_c^{(d)} = 5\,\text{MPa},\ K_{Ic}^{(d)} = 1\,\text{MPa.m}^{1/2}$.
- inclusion : $\sigma_c^{(i)} = 7.2\,\text{MPa},\ K_{Ic}^{(i)} = 1.3\,\text{MPa.m}^{1/2}$.

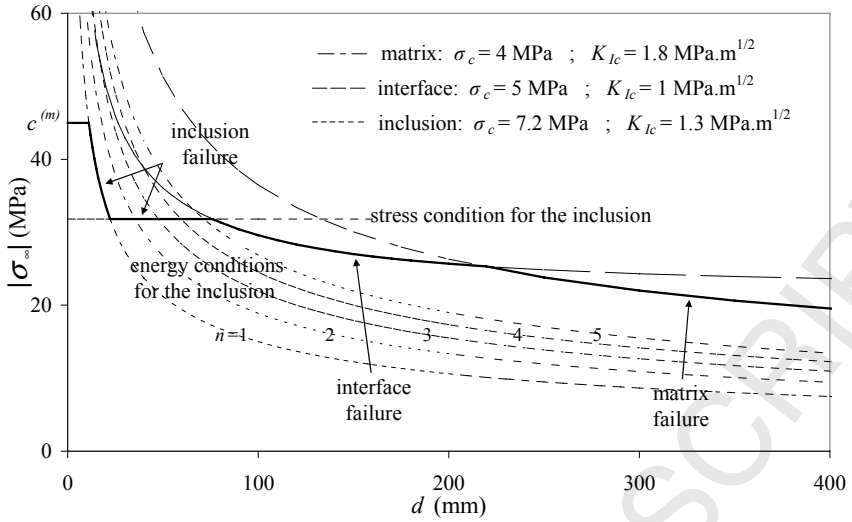

Figure 14. Critical remote load $|\sigma_\infty|$ function of the inclusion diameter d .

Different characteristic regimes are brought into evidence in figure 14.

- For very small inclusion size ($d \le 11$ mm), the matrix fails under a compressive stress because its strength $c^{(m)}$ is reached prior to any of the three other failure mechanisms.
- For small inclusion sizes ($11\,\text{mm} \le d \le 76$ mm), the single or multiple inclusion failure mechanism becomes predominant. A single crack can appear in the concretion for $11\,\text{mm} \le d \le 35$ mm, two cracks for $35\,\text{mm} \le d \le 48$ mm, three cracks for $48\,\text{mm} \le d \le 60$ mm, four cracks for $60\,\text{mm} \le d \le 71$ mm, and five cracks for $71\,\text{mm} \le d \le 76$ mm.
- For medium inclusion sizes ($76\,\text{mm} \le d \le 219$ mm), the interface debonding takes place prior to other mechanisms of failure.
- Finally for larger inclusion sizes ($d \ge 219$ mm), the matrix failure becomes the predominant mechanism.

Therefore it is clear that the naturally selected mechanism is strongly governed by the inclusion diameter.

Other combinations of material properties can lead to different conclusions (see figures 15.a to 15.e). Moreover, if the failure parameters of one of the components (i.e. matrix, inclusion or interface) are sufficiently low, the associated mechanism may completely hide the others (for example in case of a very weak matrix, its failure can occur whatever the diameter of the inclusion).

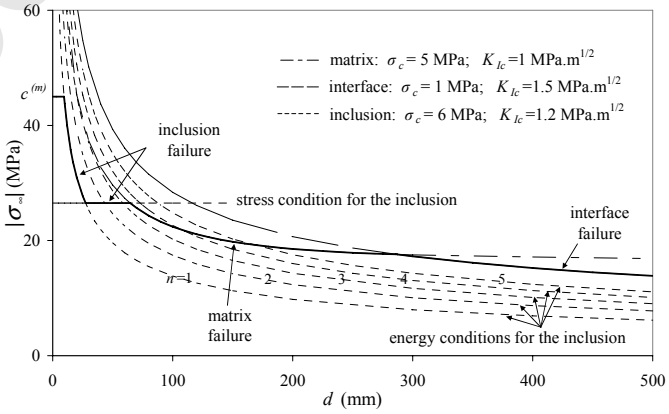

(a)

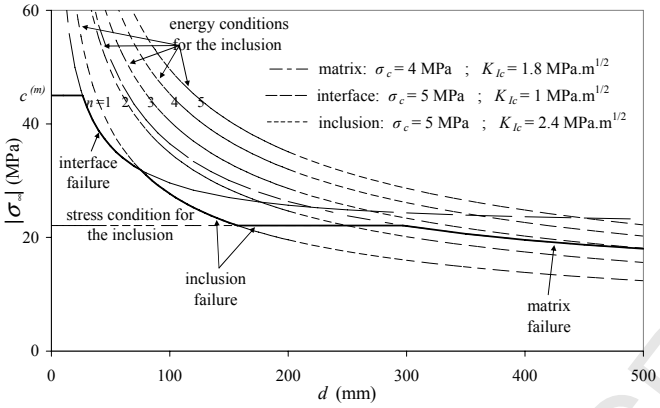

(b)

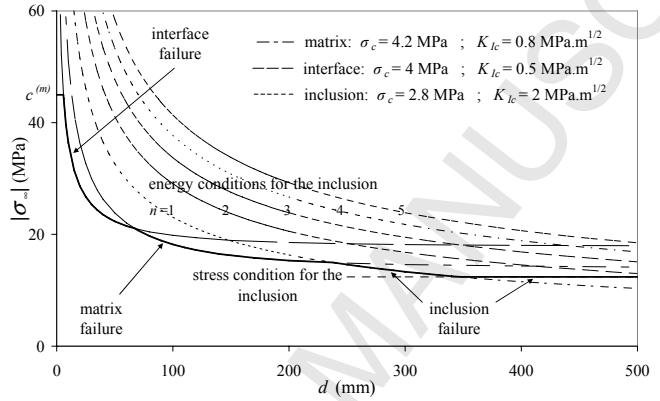

(c)

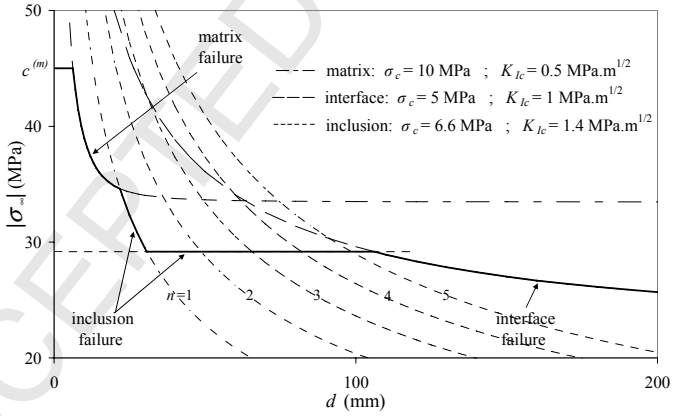

(d)

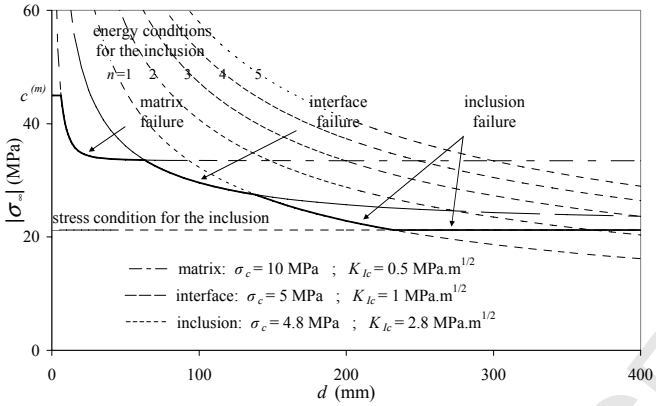

(e)

Figure 15. Various combinations of failures' parameters (inclusion, matrix and interface) allow to draw different conclusions about the influence of the concretion diameter d. A small concretion diameter leads to the inclusion failure (case (a)), to the interface failure (cases (b) and (c)), or to the matrix failure (cases (d) and (e)).

10. Conclusions

The most original part of this work is the brittle fracture model for multiple failures in the inclusion. Results have been obtained for an inclusion stiffer than the surrounding matrix as often met in sediment beds. Failure of the inclusion can occur only for a matrix Poisson ratio $\nu^{(m)} \geq 0.3$. The overburden at concretion failure is very sensitive to the value of this parameter, for $\nu^{(i)} = 0.1$, $\sigma_c^{(i)} = 5\,\text{MPa}$ and $K_{Ic}^{(i)} = 1\,\text{MPa.m}^{1/2}$, the failure load decreases by 55 % as $\nu^{(m)}$ changes from 0.3 to 0.4, whatever the inclusion size. The Poisson ratio ν_i of the inclusion has also a significant role although less pronounced. For a fixed diameter of inclusion d, $\nu^{(m)} = 0.4$, $\sigma_c^{(i)} = 5\,\text{MPa}$ and $K_{Ic}^{(i)} = 1\,\text{MPa.m}^{1/2}$, the critical load at failure increases by roughly 65 % as $\nu^{(i)}$ changes from 0.1 to 0.4.

In this model, it is assumed that almost all the extra energy is consumed by the fracture mechanisms. This is a reasonable hypothesis since, due to the confinement, the concretion pieces cannot be quickly dispersed. Any kinetic energy production is avoided except perhaps if acoustic waves emanate from the cracks' nucleation and propagate through the matrix. In that case, the predicted number of cracks within the inclusion, using this model, overestimates the actual number since part of the available energy is used for the propagation of these acoustic waves.

Acknowledgments: The authors are indebted to Institut Français du Pétrole (IFP) for its financial support.

References

Bessinger B., Cook N.G.W., Myer L., Nakagawa S., Nihei K., Benito P., Suarez-Riviera R., 2003. The role of compressive stresses in jointing on Vancouver Island, British Columbia, J. Structural Geology 25, 983-1000.

Eidelman A., Reches Z., 1992. Fracture pebbles – A new stress indicator, Geology 20, 307-310.

Eshelby J.D., 1957. The determination of the elastic field of an ellipsoidal inclusion, and related problems, Proc. of the Royal Soc. Of London 241, 376-395.

Lash G.G., Engelder T., 2007. Jointing within the outer arc of a forebulge at the onset of the Alleghanian Orogeny, J. Structural Geology 29, 774-786.

Leguillon D., 2002. Strength or toughness? A criterion for crack onset at a notch, Eur. J. Mech. A/Solids 21, 61-72.

Leguillon D., Quesada D., Putot C., Martin E., 2007. Prediction of crack initiation at blunt notches and cavities – Size effect, Engrg. Fract. Mech. 74, 2420-2436.

Leguillon D., Sanchez-Palencia E., 1987. Computation of singular solutions in elliptic problems and elasticity, Wiley, New-York, Masson, Paris.

Lorenz J.C., Teufel W.T., Warpinski N.R., 1991. Regional fracture I: A mechanism for the formation of regional fractures at depth in flat-lying reservoirs, AAPG Bulletin 75(11), 1714-1737.

Mandl G., 2005. Rock joints – The mechanical genesis, Springer Verlag, Berlin, Heidelberg.

Mc Conaughy D.T., Engelder T., 1999. Joint interaction with embedded concretions: joint loading configurations inferred from propagation paths, J. Structural Geology 21, 1637-1652.

Olson J.E., 2004. Predicting fracture swarms – The influence of subcritical crack growth and the crack-tip process zone on joint spacing in rock, in The initiation, propagation and arrest of joints and other fractures, Cosgrove J.W., Engelder T. eds., Geological Society, London, Special Publications 231, 73-87.